ACS NANO
Cite This: ACS Nano 2019, 13, 10469−10480
www.acsnano.org

ARTICLE

Dynamically Stretchable Supercapacitor for Powering an Integrated Biosensor in an All-in-One Textile System

Heun Park,[†] Jung Wook Kim,[†] Soo Yeong Hong,[†] Geumbee Lee,[‡] Hanchan Lee,[†] Changhoon Song,[†] Kayeon Keum,[†] Yu Ra Jeong,[†] Sang Woo Jin,[‡] Dong Sik Kim,[†] and Jeong Sook Ha*[,†,‡]

[†]Department of Chemical and Biological Engineering and [‡]KU-KIST Graduate School of Converging Science and Technology, Korea University, 145 Anam-ro, Seongbuk-gu, Seoul 02841, Republic of Korea

Supporting Information

ABSTRACT: **Textile-based electronics have attracted much attention as they can perfectly combine the functionality of wearable devices with the soft and comfortable properties of flexible textile fibers. In this work, we report a dynamically stretchable high-performance supercapacitor for powering an integrated sensor in an all-in-one textile system to detect various biosignals. The supercapacitor fabricated with MWCNT/MoO_3 nanocomposite electrodes and nonaqueous gel electrolyte, along the course direction of the fabric, exhibits stable and high electrochemical performance under dynamic and static deformation, including stretching in real time, regardless of the strain rate. The strain sensor created along the wale direction of the fabric shows a high sensitivity of 46.3 under an applied strain up to 60%, a fast response time of 50 ms, and high stability over 10 000 cycles of stretching/releasing. Finally, the supercapacitor and strain sensor are integrated into an all-in-one textile system *via* liquid-metal interconnections, and the sensor is powered by the stored energy in the supercapacitor. This system sewed into cloth successfully detects strain due to joint movement and the wrist pulse. This work demonstrates the high feasibility of utilizing the fabricated stretchable all-in-one textile system for real-time health monitoring in everyday wearable devices.**

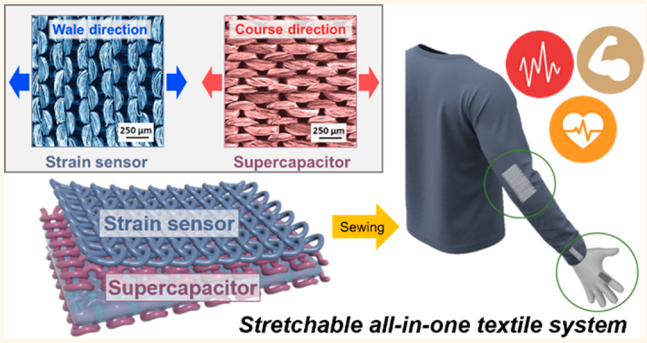

KEYWORDS: *textile electronics, all-in-one system, stretchable devices, stretchable supercapacitors, strain sensors*

In recent years, there has been a growing interest in the development of flexible/stretchable wearable electronic devices, and studies on flexible textile fibers with multielectronic functions have been actively performed.[1−5] Owing to their flexibility, special attention has been paid to textile fibers as an ideal platform for wearable electronic devices that people can feel comfortable wearing all day.[6] In the past, users have suffered from the inconvenience of wearing rigid electronic devices created *via* simple attachment onto cloth or connection with a conductive fiber. To solve this uncomfortable situation, it is necessary to develop electronic devices that can maintain the intrinsic properties of flexible fibers.[7]

Various studies on textile electronic devices, including sensors, nanogenerators, and supercapacitors, have been reported for wearable applications.[8−14] Deng's group synthesized nickel/active-material-coated flexible fibers as a simple and effective platform to fabricate strain sensors, triboelectric nanogenerators, and supercapacitors for wearable energy and sensor devices.[15] However, those fabricated strain sensors could be driven only by the external power supply through the long wire connections, which is not good for practical application as wearable devices. Thus, an effective strategy is to implement all-in-one systems for specific wearable applications that integrate energy storage devices with sensors. The Zhi group reported a new system design that combined a textile-type supercapacitor, a photodetector, and a strain sensor, eliminating the limitations on the system weight and size.[16] However, rather poor performances were observed for individual devices and systems due to the supercapacitor and strain sensor sharing electrodes.

Textiles with knitted structures can be intrinsically stretched because the meandering loops in knitted textiles can be extended in different directions. As a future energy storage

Received: June 4, 2019
Accepted: August 28, 2019
Published: August 28, 2019

DOI: 10.1021/acsnano.9b04340
ACS Nano 2019, 13, 10469−10480

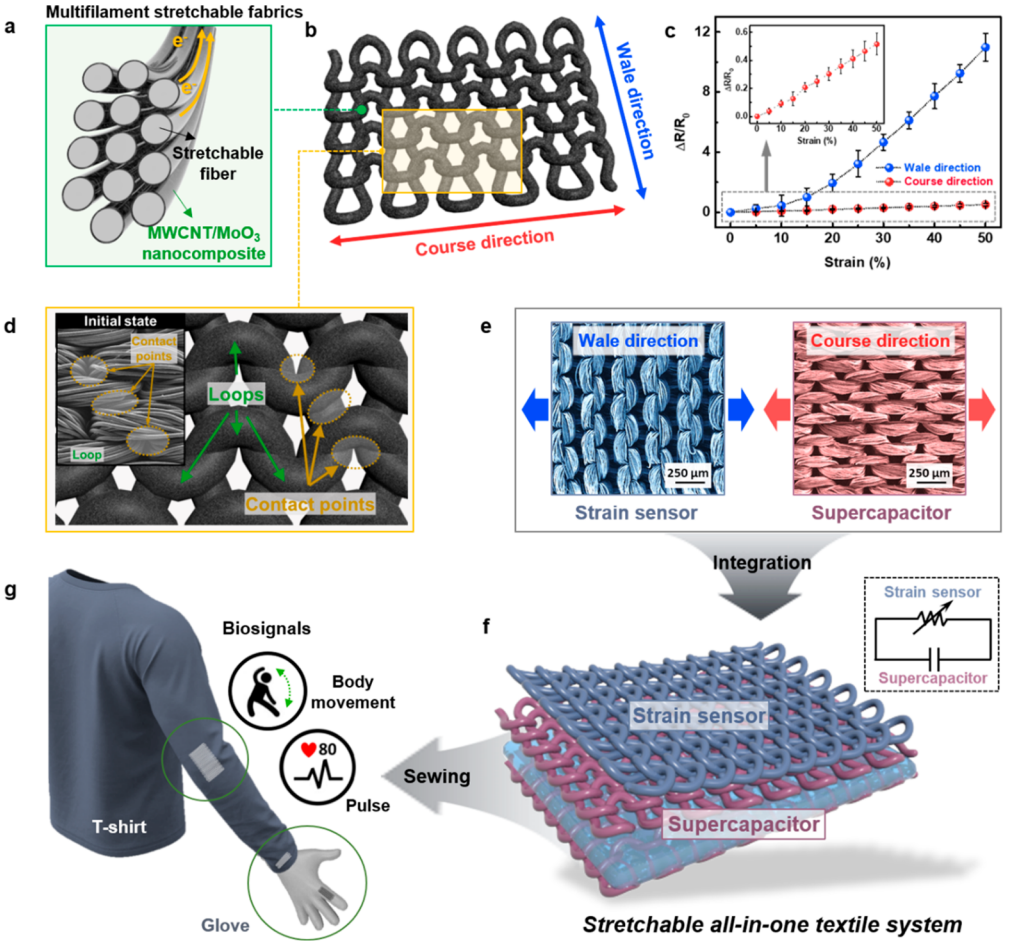

Figure 1. Schematic illustration of the fabricated stretchable all-in-one textile system. (a) High-magnification illustration of the cross section of the stretchable fiber showing the multifilament structure and MWCNT/MoO_3 nanocomposite in the fabric. (b) Schematic diagram of the wale and course directions of a knitted (purl loop) fabric. (c) Relative resistance changes *versus* strain curves for wale (blue) and course (red) direction stretching. (d) Schematic illustration of contact points between the loops in the knitted fabric structure. Inset is the SEM image of the textile. (e) SEM images showing the fabric with wale (left) and course (right) direction stretching. (f) Integration of the supercapacitor and the strain sensor. (g) Conceptual illustration of the integration system sewn onto a T-shirt and a nylon glove for biosignal monitoring.

device, supercapacitors have been extensively applied to wearable devices owing to their advantages over batteries, such as simple structure, fast charge/discharge, high power density, and excellent cycle stability.[17,18] Additionally, lightweight, flexible, and stretchable textile-based strain sensors can be worn for a long time without inconvenience to the user and are becoming a key technology in the human interface because they can continuously collect data related to breathing or body motion.[19,20]

Here, we demonstrate a stretchable all-in-one system of textile-based supercapacitors and strain sensors that can detect various biosignals. The supercapacitor and strain sensor were fabricated in two different stretching directions of the fabric. As stretchable electrodes for the high-performance supercapacitors, multiwalled carbon nanotubes (MWCNTs) and pseudocapacitive molybdenum trioxide nanowires (MoO_3 NWs) were synthesized. First, among the various carbon-based materials, carbon nanotubes (CNTs) have attracted significant interest as an excellent candidate for use in various electrochemical supercapacitors and physical sensors due to their chemical/mechanical stability, high conductivity, and large specific surface area. MoO_3 also has attracted considerable interest as a pseudocapacitive material in addition to its low cost, nontoxicity, high electrochemical activity, and environmentally friendly properties.[21,22] Due to the low conductivity of MoO_3, however, the hybrid composite of MWCNTs and MoO_3 NWs was used for high-performance supercapacitors in this work. In addition, the sensitivity of the strain sensor could be easily controlled by the mixing ratio of MoO_3 NWs. The fabricated supercapacitors exhibited high capacitance and cycle stability and showed mechanical stability under various deformation conditions, such as static and dynamic folding, twisting, and stretching. The strain sensor made of the same MWCNT/MoO_3 NW materials exhibited a high sensitivity, with stable and reproducible performance and a fast response time. The all-in-one system was sewn on clothes, and the strain sensor was powered by the stored energy of the supercapacitor and could detect the movements of fingers, wrists, and elbow joint as well as the wrist pulse. This work suggests the high application potential of our stretchable all-in-one textile system for various fields including rehabilitation, healthcare, sports, and medical treatments as a next-generation wearable device.

DOI: 10.1021/acsnano.9b04340
ACS Nano 2019, 13, 10469−10480

RESULTS AND DISCUSSION

We report the fabrication of a dynamically stretchable all-in-one textile system consisting of a supercapacitor and a strain sensor for monitoring biosignals, where the sensor is driven by the stored energy of the integrated supercapacitor without the use of wire connections to an external power supply. Such a key advance includes a deliberate selection of suitable materials and a design rule of individual high-performance devices in two different stretching directions of the textile: a supercapacitor in the course direction but the strain sensor in the wale direction. Through deliberate control of single active materials of a MWCNT/MoO_3 NW nanocomposite and careful selection of stretching directions of the textile for fabricating individual devices, a dynamically stretchable all-in-one textile system is easily fabricated. The fabricated all-in-one sensor system with liquid metal interconnections is sewn on clothes, detecting the movements of fingers, wrists, elbow joints, and the wrist pulse. The fabricated stretchable all-in-one textile system is schematically shown in Figure 1. The conductive fabric was made *via* spray-coating the MWCNT/MoO_3 NW nanocomposite onto stretchable fabric with a multifilament structure, as shown in Figure 1a. Fabric textile networks with a knitted structure can withstand tensile deformation in the vertical and horizontal directions but exhibit different tensile properties.[23] Course is defined as a series of horizontally connected loops, and wale is a series of vertically intermeshed loops, as given in Figure 1b.[24,25] Figure S1a shows an optical image of the stretchable fabric substrate (nylon 82%/Spandex 18%) we used. The thickness of the fabric substrate was estimated to be approximately 300 μm based on the cross-sectional scanning electron microscopy (SEM) image in Figure S1b. Initially, we tried the dip-coating process. To uniformly coat the fabric, the fabric was sufficiently immersed in the coating solution for 5 min and then dried in a 65 °C oven for 15 min. SEM images were taken from the dip-coated fabric, as shown in Figure S2. The dip-coating showed a uniform coating without noticeable agglomeration. However, we obtained a high resistance value of 8.55 MΩ despite the 15 cycles with the long times of more than 5 h for each sample. After 10 cycles, the resistance did not change significantly, as shown in Figure S3. In addition, the fabric exhibited poor conductivity and was insufficient for use as a conductor, suggesting that the dip-coating method should not be successful. Spray-coating was selected for fabricating conductive fabric substrates because of the advantages of this process, such as low cost, high speed, simplicity, and uniformity over large areas, which are good properties for manufacturing conductive layers on complex nonplanar surfaces.[26,27] The MWCNT/MoO_3 nanocomposite solution was spray-coated at a 90° angle above the stretchable fabric substrate while the substrate was heated at 80 °C, as schematically shown in Figure S4.

Applied strain is defined as $\varepsilon = (l - l_0)/l_0 \times 100$, where l_0 and l are the distances between the fixed edges before and after being stretched, respectively.[28,29] Figure 1c shows the changes in the resistance for stretching in both the wale and course directions. Ten milliliters of a MWCNT solution dispersed in ethanol was spray-coated onto a stretchable fabric substrate. The conductive fabric exhibited a positive piezoresistivity effect, where the resistance increased with the decrease in percolation in the wale direction;[30] a 20-fold higher change in the relative resistance was observed at an applied strain of 50% compared to that observed with stretching in the course direction. There was a slight change in the resistance upon application of strain in the course direction, as shown in the inset of Figure 1c.

Figure 1d shows the schematic illustration of the knitted structure where conductive fabric loops contact adjacent loops next to each other. When the coated fabric is stretched, the resistance changes with deformation. The change in resistance of the knitted fabric with applied strain can be explained following the equation of Holm's contact theory (1):[31,32]

$$R_C = \frac{\rho}{2}\sqrt{\frac{\pi H}{nP}} \tag{1}$$

where ρ, n, P, and H are the resistivity of the fiber, the number of contact points, the contact pressure, and the material hardness, respectively. The material hardness and electrical resistivity remain constant, and the number of contact points and the contact pressure change with the applied strain. Thus, higher contact pressure and the increased number of contact points reduce the contact resistance. In this knitted structure, contact pressure between the loops has a maximum value before stretching and uniaxial stretching reduces the number of contact points between the loops.[33,34] Hence, the contact pressure and the number of contacting points between loops become smaller with the applied strain. As a result, the overall electrical resistance of the fabric increases with strain due to the increase of contact resistance. The SEM images taken from the fabric before and after stretching by 30% in the course direction are shown in Figure S5. No crack is observed in the 30% stretched state. Thus, we consider that the resistance change is not caused by cracking but by the deformation of the structure with the change of the contact resistance.

To analyze and understand the change in resistance with respect to the applied strain, the change in the textile morphology was investigated in both the wale and course directions. The change in resistance along the wale direction is much larger than that along the course direction. It is attributed to the different deformation characteristics along the two directions, as shown in Figure S6. Contact points between loop and loop still remain in the course direction stretching (Figure S6a), while the separation of contact points is significantly increased with the stretching in the wale direction (Figure S6b). As the space between neighboring loops increased, the change in resistance was reported to increase.[35] As a result, the resistance variation in the wale direction is larger than that in the course direction under the same stretching condition. Figure 1e shows SEM images taken from the MWCNT-coated fabric substrate under 50% stretching in the wale and course directions. The change in the resistance is maximized under stretching in the wale direction, whereas it is minimized under stretching in the course direction. Thus, we can fabricate the stretchable strain sensor and supercapacitor along the corresponding directions. Both the supercapacitor and the strain sensor were made of a single active material of a MWCNT/MoO_3 nanocomposite.

Based upon those preliminary investigations, we developed a stretchable, textile all-in-one system *via* stacking and connecting these two devices, as shown in Figure 1f. The strain sensor can be driven by the stored power of the supercapacitor. Finally, the stretchable, textile all-in-one system was sewn onto cloth and was detached from the cloth by washing and sewn again after washing to solve the washing

DOI: 10.1021/acsnano.9b04340
ACS Nano 2019, 13, 10469−10480

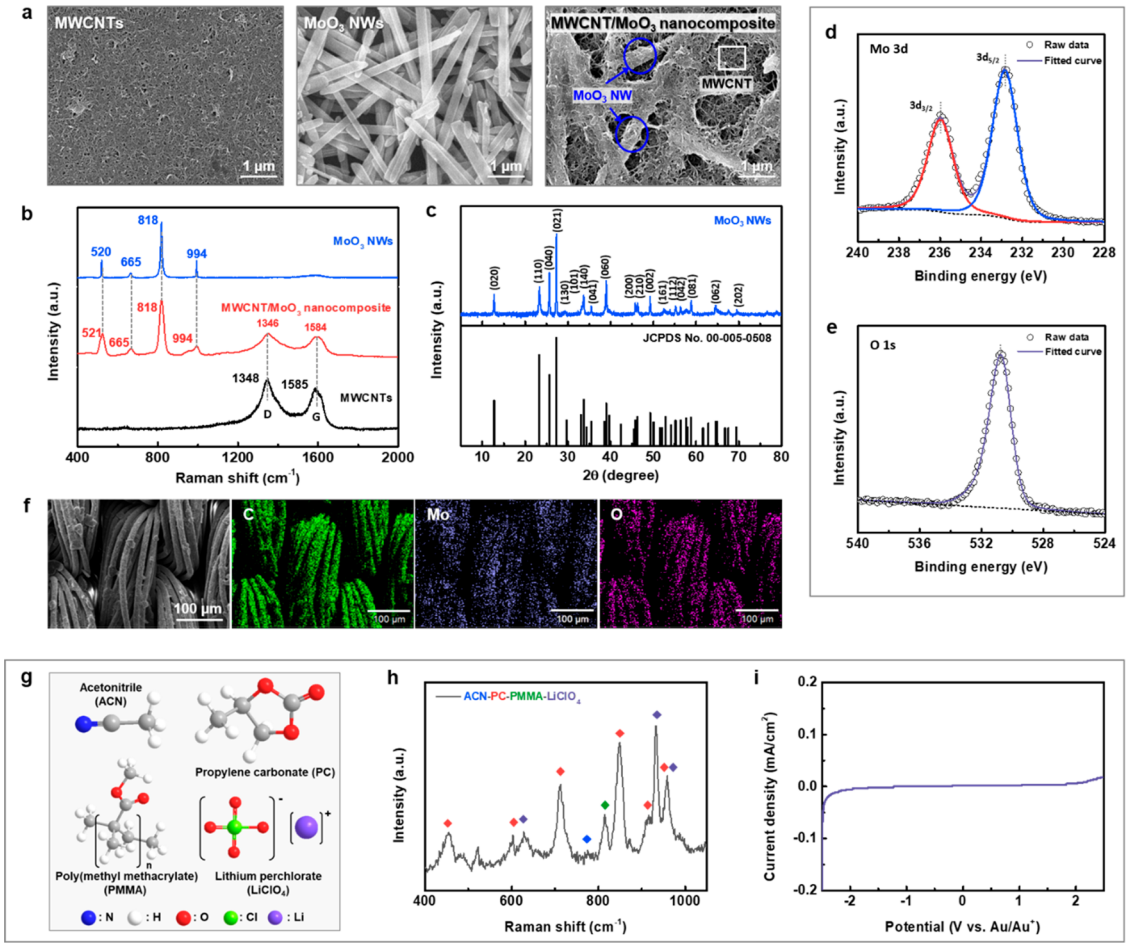

Figure 2. (a) SEM images of MWCNTs (left), MoO_3 NWs (middle), and MWCNT/MoO_3 nanocomposite (right). (b) Raman spectra of MoO_3 NWs (blue), MWCNT/MoO_3 nanocomposite (red), and MWCNTs (black). (c) XRD pattern of MoO_3 NWs. XPS spectra of (d) Mo 3d and (e) O 1s for MoO_3 NWs. (f) SEM image and EDS spectrum of the fabric uniformly covered with the MWCNT/MoO_3 nanocomposite. (g) Molecular structures of the component materials of the gel electrolyte. (h) Raman spectrum of ACN−PC−PMMA−$LiClO_4$. (i) Linear sweep voltammetry of the gel electrolyte recorded using two gold electrodes at a scan rate of 5 mV/s.

problems. It is used to detect the movement of joints and the wrist pulse, as shown in Figure 1g.

The morphology and chemical structures of the materials synthesized to create the electrodes and electrolytes are shown in Figure 2. Figure 2a shows the SEM images taken from the functionalized MWCNTs, high-purity MoO_3 NWs synthesized by a hydrothermal processes, and the MWCNT/MoO_3 nanocomposite. The MWCNT/MoO_3 nanocomposite was uniformly blended. Typical Raman spectra of the synthesized materials are shown in Figure 2b. In the spectrum of the MWCNT/MoO_3 nanocomposite, the peak at 994 cm^{-1} is assigned to antisymmetric $\nu_{as}(Mo{=}O)A_g$ stretching, and the strong band at 818 cm^{-1} represents symmetric $\nu_s(Mo{-}O_3{-}Mo)A_g$ stretching. The peaks at 665 and 521 cm^{-1} are ascribable to the antisymmetric $\nu_{as}(Mo{-}O_2{-}Mo)B_{2g}$ stretching and bending modes, respectively. Two prominent peaks for MWCNTs appear at 1348 cm^{-1} (D band) and 1585 cm^{-1} (G band).[28,36] The X-ray diffraction (XRD) pattern of the MoO_3 NWs is shown in Figure 2c. The peaks appearing at 2θ values of 12.74, 25.69, 27.31, 33.13, 33.67, 35.47, 38.95, 46.30, 55.22, 56.37, and 58.85° correspond to the (020), (040), (021), (101), (140), (041), (060), (210), (112), (042), and (081) planes of the orthorhombic crystal structure of MoO_3, respectively. The polycrystalline MoO_3 peaks in the XRD pattern confirm a = 3.96 Å, b = 13.85 Å, and c = 3.69 Å in accordance with the JCPDS card no. 00-005-0508.[37] Figure 2d,e shows the X-ray photoelectron spectroscopy (XPS) spectra of the synthesized MoO_3 NWs. The Mo 3d core level spectrum of MoO_3 shows a spin−orbit doublet at 236.0 and 232.9 eV for Mo $3d_{3/2}$ and Mo $3d_{5/2}$, confirming the +6 oxidation state of Mo (Figure 2d). The energy difference between the doublet peaks is 3.1 eV for MoO_3.[38,39] The O 1s core level spectrum of MoO_3 in Figure 2e shows a peak at 530.7 eV that can be attributed to the presence of oxygen in Mo−O−Mo bonding. This result confirms the −2 oxidation state of oxygen.[37,40] Energy-dispersive spectroscopy (EDS) images show the uniform distribution of the MWCNT/MoO_3 nanocomposite on the fiber surface, as shown in Figure 2f. The SEM images also confirmed that the synthesized material was uniformly coated on the fabric substrate, as shown in Figure S7. We synthesized a nonaqueous solvent-based ACN−PC−PMMA−$LiClO_4$ electrolyte for high operational cell voltage and air/mechanical stability. Our fabricated organic electrolyte consists of acetonitrile (ACN), propylene carbonate (PC), lithium perchlorate ($LiClO_4$), and poly(methyl methacrylate) (PMMA), where ACN and PC act as organic solvents, $LiClO_4$ both as conducting salt and reactant to undergo pseudocapacitive reaction with molybdenum trioxide, and PMMA as a

DOI: 10.1021/acsnano.9b04340
ACS Nano 2019, 13, 10469−10480

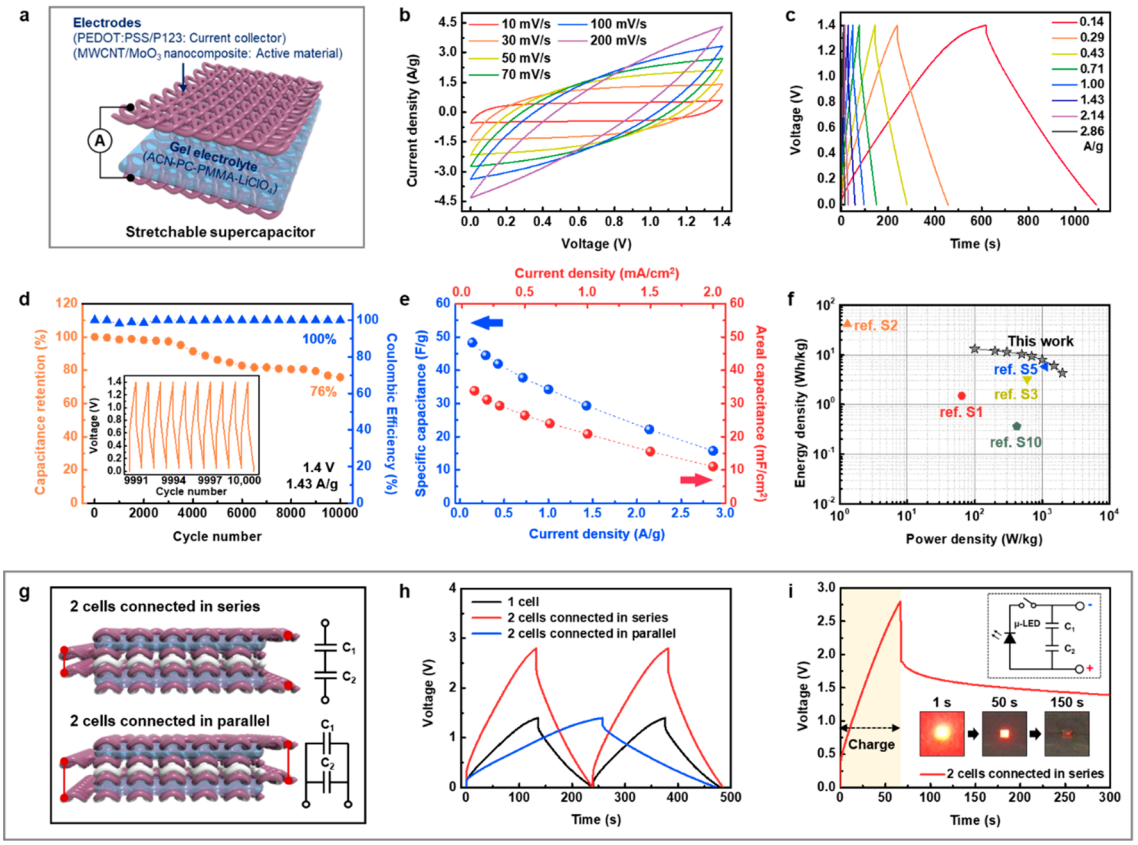

Figure 3. Electrochemical performance of a supercapacitor consisting of MWCNT/MoO_3 nanocomposite electrodes and a gel electrolyte. (a) Schematic illustration of the fabricated stretchable supercapacitor. (b) CV curves obtained at scan rates of 10, 30, 50, 70, 100, and 200 mV/s. (c) GCD curves obtained at a current density from 0.14 to 2.86 A/g. (d) Capacitance retention (orange) and Coulombic efficiency (blue) for charge/discharge cycles at a current density of 1.43 A/g. (e) Specific and areal capacitances with variation of current density. (f) Ragone plot. (g) Schematic illustration of two supercapacitors connected in series and parallel with circuit diagrams. (h) GCD profiles of the supercapacitor arrays connected in series and parallel. (i) Charge/discharge behaviors of two serially connected supercapacitors. The bottom optical images are of a μ-LED powered by the connected supercapacitors with the elapsed time after charging.

polymerizing agent to immobilize and to add viscosity to the electrolyte. Typically, aqueous electrolytes have limited operation voltage below 1 V due to the electrochemical decomposition voltage of water. In addition, the evaporation of water under ambient air conditions results in capacitance degradation due to the reduction in ion mobilities by evaporation of water.[41] As a result, we used the gel-type ACN−PC−PMMA−$LiClO_4$ electrolyte owing to many advantages including the easy processing, good mechanical strength, a wide operation voltage window, and air stability for the supercapacitor performance. Although ACN, PC, and $LiClO_4$ are known to be toxic based on material safety data sheets, these organic solvents and conducting salts are commonly used as an electrolyte material for high-performance supercapacitors and electrochromic devices.[42,43] More importantly, our organic solvent-based electrolyte is gel-type and has high viscosity. We measured shear viscosity of the gel electrolyte through a rheometer, which was about 7600 times higher than that of deionized (DI) water at a high shear rate of 100, as shown in Figure S8. Thus, the electrolyte is in an almost solid state so that it does not flow, not directly contacting the skin through the fabric. The electrolyte is also located between the electrodes, and the supercapacitor is sewn on the fabric for biosignal measurement. Therefore, the devices do not directly touch the skin. Even when measuring pulse, the strain sensor is located at the top of the all-in-one system, making it difficult to contact the skin.

Figure 2g,h shows the molecular structures of the individual components and the Raman spectrum of the ACN−PC−PMMA−$LiClO_4$ gel electrolyte. Raman bands associated with each component are clearly observed, and the blue, red, green, and purple diamonds correspond to ACN, PC, PMMA, and $LiClO_4$, respectively. The strong Raman band at 712 cm^{-1} can be assigned to the deformation of a locally symmetric PC ring, and the pentagonal ring of PC can be deformed by interacting with Li^+ ions dissolved in the solvent. The asymmetric C−C≡N bending mode of ACN is located at 776 cm^{-1}. The bands at 916 and 959 cm^{-1} are inherent to PC, and the 931 cm^{-1} band can be assigned to a solvent-shared ion pair (Li^+−PC−ClO_4^-).[41,43] The 813 cm^{-1} band is assigned to a stretching mode of the ester side chain group of PMMA.[44] A linear sweep voltammetry curve was taken to investigate the electrochemical stability window (ESW) of the synthesized electrolyte, as shown in Figure 2i, and this test checks for the possible decomposition of constituent materials of the electrolyte over a wide potential range.[45] The ESW of the ACN−PC−PMMA−$LiClO_4$ electrolyte was found to be from −2.5 to 2.5 V in a cell consisting of symmetric gold electrodes. The current density remained almost zero during scanning at a scan rate of 5 mV/s, indicating no decomposition of the components within this potential range.

DOI: 10.1021/acsnano.9b04340
ACS Nano 2019, 13, 10469−10480

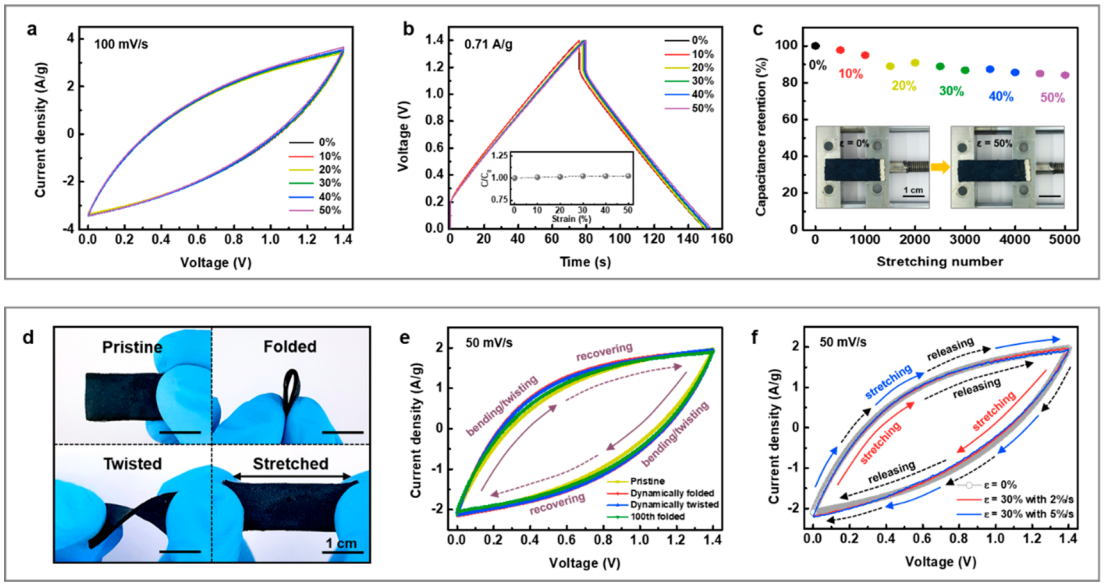

Figure 4. Electrochemical performance of the supercapacitor measured under real-time static stretching and dynamic deformation/stretching. (a) CV curves under stretching measured at a scan rate of 100 mV/s. (b) GCD curves under stretching at a current density of 0.71 A/g. The inset shows the normalized capacitance (C/C_0). (c) Capacitance retention as a function of stretching/releasing cycle number under different strains. The inset shows the optical images of the supercapacitor before (left) and after (right) stretching. (d) Optical images and (e) CV curves of the supercapacitor measured during various dynamic deformation: pristine, folding, twisting, and after 100 folding cycles. (f) CV curves measured during dynamic stretching/releasing cycles at 30% strain with different strain rates of 2 and 5%/s. Here, the CV curves without applied strain (ε = 0%) are gray.

Before the fabrication of a stretchable fabric supercapacitor, the electrochemical performance of the MWCNT/MoO_3 nanocomposite electrode was evaluated in a three-electrode system using a 0.5 M $LiClO_4$ aqueous solution as the liquid electrolyte, Pt wire as the counter electrode, and Ag/AgCl as the reference electrode. With a fixed amount of MWCNTs (3 mL) on the ITO/PET film, the volume fraction of MoO_3 NWs was varied, as described in Figure S9a. Galvanostatic charge−discharge (GCD) curves were obtained with different volume fractions of MoO_3 NWs (Figure S9b), and the calculated capacitance was found to increase with the volume fraction up to 0.25 but then decreased, as shown in Figure S9c. With a volume fraction of 0.25, the capacitance dramatically increased by approximately 3 times due to the redox reaction between the MoO_3 NW surface and Li^+ ions in the aqueous electrolyte.[46] However, as the volume fraction of MoO_3 NWs further increased, the capacitance decreased due to the increase in the sheet resistance (R_{sh}), as shown in Figure S10. Figure S11 shows the SEM images of the electrodes with different volume fractions of MoO_3 NWs.

Figure 3 shows the electrochemical performance of a stretchable fabric supercapacitor with the MWCNT/MoO_3 nanocomposite electrode and ACN−PC−PMMA−$LiClO_4$ electrolyte. Figure 3a is a schematic illustration of the fabricated supercapacitor. First, the change in the resistance when strain was applied to the fabric substrate was measured with various MWCNT/MoO_3 nanocomposite solutions. As the amount of coated MWCNT/MoO_3 nanocomposite increased, the change in the resistance decreased (Figure S12a). Second, to obtain a high-performance supercapacitor, we dip-coated a stretchable conductor of the PEDOT:PSS/P123 composite to create the current collector of the fabric electrode for improved conductivity. With an increase in the number of dip-coating cycles, the resistance dramatically decreased, as shown in Figure S12b. Such a change in resistance was also investigated with and without the PEDOT:PSS/P123 composite current collector when 10 mL of MWCNT/MoO_3 nanocomposite solution was coated on the substrate, as shown in Figure S13a. Without the current collector, an approximately 8.6 times greater change in resistance was observed at an applied strain of 60%. This result confirmed that the fabricated supercapacitor is more mechanically stable with a current collector under stretching deformation. The thickness of the supercapacitor fabricated with the optimal synthesized materials was estimated to be ~940 nm based on the cross-sectional SEM image in Figure S13b. After dip-coating of the stretchable fabric with PEDOT:PSS/P123, the MWCNT/MoO_3 nanocomposite was spray-coated on it. Thus, there is just a physical interaction between the two layers. In order to check the adhesion, we did the 3M Scotch tape test, as shown in Figure S14. After the attachment/detachment of the Scotch tape, there was no material on the tape, confirming the good adhesion between two layers. Figure S15 shows the cyclic voltammetry (CV) curves measured at a scan rate of 50 mV/s. The fabricated supercapacitor could be operated at different voltages, ranging from 1.0 to 2.0 V. The maximum and minimum current values in the CV curves were symmetric at 1.4 V, indicating the stability of the ACN−PC−PMMA−$LiClO_4$ gel electrolyte. Therefore, the potential of 1.4 V was selected as the stable operating voltage of our supercapacitor. The capacitance is mainly caused by the adsorption/desorption of Li^+ ions onto/from the MoO_3 NWs. The charge storage mechanism can be explained by the following eq 2:[46]

$$MoO_3 + xLi^+ + xe^- \leftrightarrow Li_xMoO_3 \quad (2)$$

As shown in Figure 3b and Figure S16a, the CV curves show symmetric charge/discharge current levels and quasi-rectangular shapes at various scan rates up to 200 mV/s. The GCD curves were taken at current densities ranging from 0.14 to

DOI: 10.1021/acsnano.9b04340
ACS Nano 2019, 13, 10469−10480

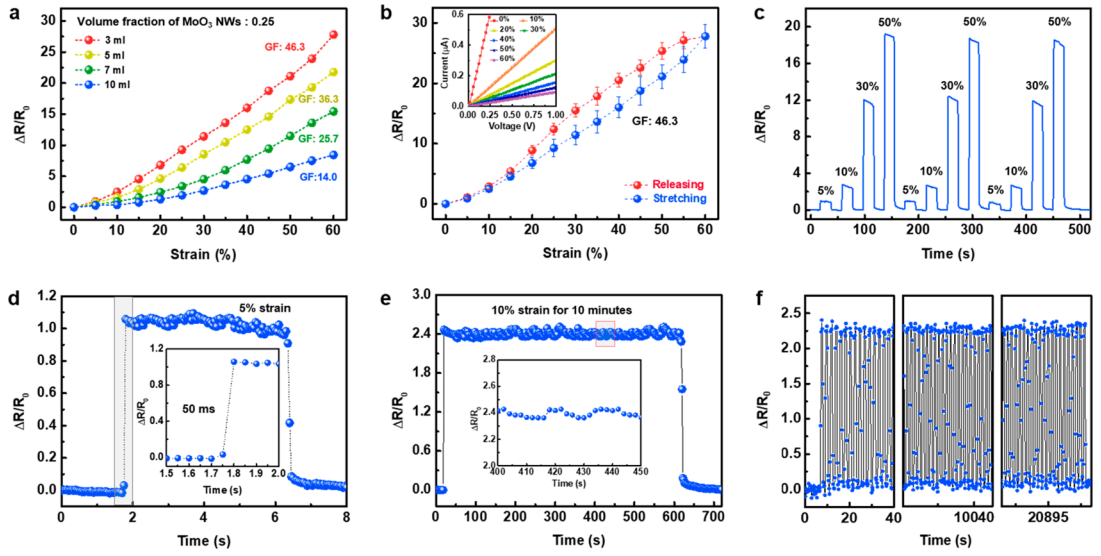

Figure 5. Electromechanical properties of the stretchable strain sensor. (a) Relative resistance changes *versus* strain curves with various volumes of coating solutions at a fixed volume fraction of MoO_3 NWs of 0.25. (b) Relative change in the resistance of the strain sensor *versus* the applied strain. (c) Repetitive measurements of the change in the relative resistance of the sensor with the variation of strain in a sequence of 5, 10, 30, and 50%. (d) Response curve of the strain sensor with an applied strain of 5% showing a response time of 50 ms. (e) Characteristic of the sensor under a constant strain of 10% applied strain for 10 min. (f) Change in the relative resistance of the sensor for 10 000 stretching/releasing cycles with 10% strain.

2.86 A/g and show symmetric triangular shapes in Figure 3c. Figure 3d presents the changes in capacitance over 10 000 repetitive charge/discharge cycles at a current density of 1.43 A/g. A Coulombic efficiency (η) of 100% was maintained while the capacitance retention was approximately 86 and 76% of the initial capacitance after 5000 and 10 000 charge/discharge cycles, respectively, which were obtained by continuous operation for 5 days. In addition, cyclic stability was demonstrated with no significant distortion in the GCD curves around the 10000th cycles (inset of Figure 3d). The performance is superior to that of other recently reported flexible/stretchable/fabric supercapacitors, as shown in Table S1. Figure S16b shows the time-dependent impedance spectra (the Nyquist plot) taken over a frequency range from 1 MHz to 0.01 Hz with an amplitude of 0.01 V. In the inset of Figure S16b, the ESR value is estimated to be 83.6 Ω. The specific and areal capacitance of our supercapacitor was calculated from the GCD curves with respect to the current densities, as shown in Figure 3e. The maximum specific and areal capacitances were estimated to be 48.3 F/g and 33.8 mF/cm^2 at a current density of 0.14 A/g and 0.1 mA/cm, respectively. The maximum volumetric capacitance of our supercapacitor was also calculated to be 0.41 F/cm^3 at a current density of 1.2 mA/cm^3 in Figure S16c. More detailed specification of the fabricated supercapacitor is shown in Figure S17. In the Ragone plot in Figure 3f, the specific energy density ($E_{cell,s}$) and specific power density ($P_{cell,s}$) of our supercapacitor are calculated from the GCD curves. The supercapacitor exhibited an $E_{cell,s}$ of 13.15 Wh/kg at a $P_{cell,s}$ of 100 W/kg and a $P_{cell,s}$ of 2000 W/kg at an $E_{cell,s}$ of 4.28 Wh/kg. These energy and power densities are also comparable or superior to those of recently reported flexible/stretchable/fabric supercapacitors, as demonstrated in Table S1. Figure 3g schematically illustrates two supercapacitors connected in series and parallel with equivalent circuit diagrams. The operating voltage and capacitance could be adjusted in this way. The corresponding GCD and CV curves are shown in Figure 3h and Figure S18a, respectively. Two serially connected supercapacitors exhibit an output voltage of 2.8 V, which is twice that of a single supercapacitor. Two supercapacitors connected in parallel have a 2-fold longer discharge time than a single supercapacitor. After two serially connected supercapacitors were charged to 2.8 V, a μ-LED with a turn-on voltage of 1.6 V was turned on for 150 s, as shown in Figure 3f. Self-discharge behavior is an important concern for the practical application of supercapacitors.[45] We obtained a self-discharge curve, as shown in Figure S18b. When a single supercapacitor was fully charged to 1.4 V at a current density of 0.36 A/g, it took 4.2 h for the voltage to decrease to 0.6 V.

We confirmed the electrochemical stability of our fabric supercapacitor under mechanical deformation in both static and dynamic modes, as shown in Figure 4. The CV and GCD curves in Figure 4a,b show no noticeable change upon application of a strain up to 50% at a scan rate of 100 mV/s and current density of 0.71 A/g. The gel electrolyte did not flow out, and we could perform a deformation test without encapsulation of the supercapacitor. The inset of Figure 4b shows that the normalized capacitance remained unchanged. Furthermore, the capacitance retained ∼80% of its initial value even after 5000 stretching/releasing cycles of the application of steadily increasing strain from 10 to 50%. The inset shows the optical images of the supercapacitor in the released and 50% stretched states. Such degradation seems to originate from the slight fracture of the entire device, including the gel electrolyte, and delamination of the electrode materials under repeatedly applied strain.[45] Next, we investigated the electrochemical performance under the application of dynamic deformation. Figure 4d shows optical images of the folded, twisted, and stretched supercapacitor. Figure 4e displays the dynamically recorded CV curves at a scan rate of 50 mV/s with pristine, folding, and twisting and after 100 cycle of folding. The CV curves exhibit complete recovery of the initial performance regardless of the deformation. Figure 4f shows the CV curves taken under 30% dynamic stretching at strain rates of 2%/s

DOI: 10.1021/acsnano.9b04340
ACS Nano 2019, 13, 10469−10480

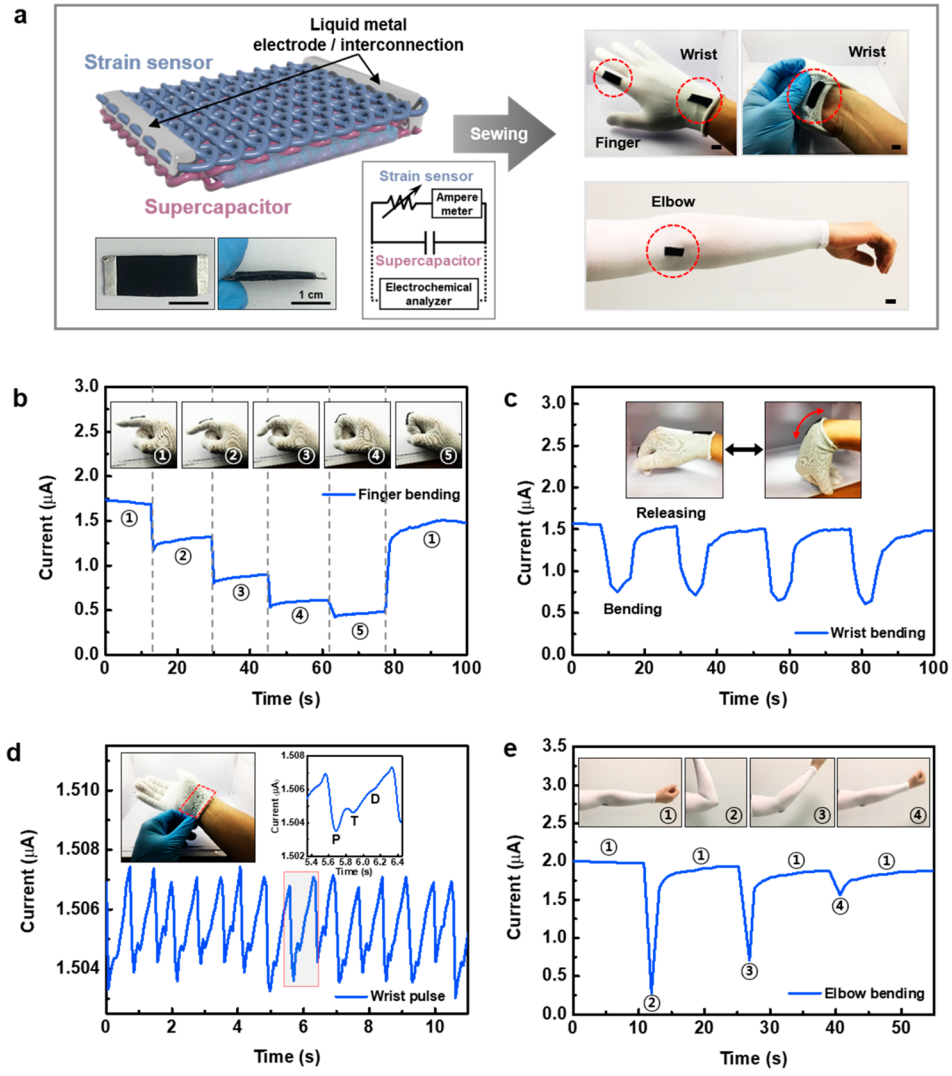

Figure 6. (a) Schematic illustration and optical images of the fabricated strain sensor and supercapacitor with a circuit diagram of the integrated system (left). Integrated all-in-one system sewn onto a T-shirt and a nylon glove. Detection of biosignals with the strain sensor driven by a supercapacitor. Current change with (b) finger bending, (c) wrist bending, (d) wrist pulse, and (e) elbow bending.

(red) and 5%/s (blue). Two and five stretching/releasing cycles are represented in the CV curves. All of the CV curves dynamically recorded under an applied strain overlap with the CV curve taken prior to the dynamic stretching. Figure S19 shows the temperature-dependent capacitance values, and a slight increase in capacitance by 0.005 $°C^{-1}$ is observed in the temperature range between 25 and 45 °C, indicating the thermal stability of our supercapacitor.[47] This result clearly confirmed that the initial capacitance is maintained under dynamic stretching regardless of the strain rate and temperature change, suggesting the high application potential of our supercapacitor for skin-attachable electronics as dynamically stretchable energy storage devices.

To optimize the performance of the strain sensor, the MoO_3 NW volume fraction was changed from 0 to 0.75 with a fixed total coating volume. Figure S20a shows that the sheet resistance increased with the increasing volume fraction of MoO_3 NWs. The change in the resistance with the volume fraction of MoO_3 NWs is shown in Figure S20b. When the volume fraction of the MoO_3 NWs was 0.25, the resistance change with 60% strain was the highest. However, the resistance change could only be measured up to 35% strain with a volume fraction of 0.5, and the electrical connection was broken even at 5% strain with a volume fraction of 0.75. This difference is attributed to the dramatic reduction in the conductive pathway through MWCNTs, and when we fabricated the strain sensor with spray-coated MoO_3 NWs only, the initial resistance was very high at 66 MΩ, as shown in Figure S21. Upon 5% strain, there appeared no current flow. Therefore, a volume fraction of 0.25 was chosen for fabricating our strain sensor.

The electrical performance of the fabricated strain sensor is shown in Figure 5. With variations in the total amount of the coating solution, the relative change in resistance with respect to the applied strain was measured and is shown in Figure 5a. Spray-coating 3 mL of solution resulted in the greatest change in resistance with applied strain, which is probably due to less percolation of conductive MWCNTs with less spray-coating solution; this result is consistent with the highest resistance being obtained with the smallest amount of coating solution in Figure S20c. The thickness and final mass loading of the optimally synthesized MWCNT/MoO_3 nanocomposite for the strain sensor are estimated to be ~570 nm from the cross-

DOI: 10.1021/acsnano.9b04340
ACS Nano 2019, 13, 10469−10480

sectional SEM image in Figure S20d and 0.4 mg/cm^2 with a high-resolution analytical balance, respectively.

The gauge factor (GF) for determining the sensitivity of the sensor can be calculated by eq 3:[48,49]

$$\mathrm{GF} = \frac{\frac{\Delta R}{R_0}}{\varepsilon} \tag{3}$$

where ΔR, R_0, and ε correspond to the change in the resistance, the initial resistance (the resistance before extension), and the applied strain, respectively. There are two slopes with variation of the amount of coating solution. It is attributed to the temporary deformation of the textile, and it appears as a plateau at low strains.[23,50] We calculated the gauge factor (slope) using the end point values at 0 and 60%. In the case of the strain sensor fabricated with 3 mL of the coating solution, the highest gauge factor of 46.3 at up to 60% strain was obtained with a high R^2 value of 0.989, indicating the good linearity, as shown in Figure 5a. So, we compared the sensitivity for the strain ranging from 0 to 60% in this work. With the strain sensor, stretching/releasing cycles were measured up to 60% strain, as shown in Figure 5b. Here, the error bars were obtained from five different sensors to confirm reproducibility. Slight hysteresis was observed during the release, and such hysteresis is reported to be mainly due to friction and structural changes in the fabric.[50] Table S2 shows that our strain sensor exhibits a superior performance compared to that of other previously reported stretchable fabric strain sensors. The inset graph shows the $I-V$ characteristics of the fabricated sensor with linear and ohmic behavior. As strain is applied, the amount of current flowing through both electrodes is reduced. In order to see the effect of washing on the strain sensor, we compared the performance of our strain sensor with and without PDMS coating after washing cycles in water. In Figure S22a, the relative resistance change of the sensor was examined after washing in DI water from 1 to 10 cycles, with and without PDMS coating. It is clearly seen that the PDMS coating protects the sensor from increasing the resistance during the washing cycles owing to the prevention of detaching the coating material by washing. In contrast, there was a dramatic increase of the resistance without PDMS coating. Even though the PDMS coating enables the stability of the sensor over washing, the sensitivity of the sensor was observed to be dramatically reduced after the PDMS coating in Figure S22b. Here, the GF decreased from 46.3 to 0.4. Thus, we did not have PDMS coating for protecting the sensor from water in this work. Figure 5c shows that the strain sensor has excellent reliability during the repetitive cycles of four sequential strains of 5, 10, 30, and 50%. A fast response to the applied strain was also observed, and the response time was estimated to be 50 ms under an applied strain of 5%, as shown in Figure 5d. Furthermore, stable strain sensing without any electrical drift was observed for over 10 min under a constant applied strain of 10% (Figure 5e). Finally, the good durability of the fabricated sensor was confirmed by repeating 10 000 cycles of 10% strain (Figure 5f). These results demonstrate that our fabricated sensor exhibits very stable and reproducible performance. In Figure S23, the temperature coefficient of resistance of this strain sensor is estimated to be −0.0038 °C^{-1} because both MWCNTs and MoO_3 NWs have a negative temperature coefficient and exhibit a decrease in resistance with an increase in temperature.[51,52] Therefore, our strain sensor will not be affected by changes in temperature, which is good for application as a skin-attachable device.

To evaluate the practical application in all-in-one wearable sensor systems, the supercapacitor and strain sensor were stacked and electrically connected *via* liquid-metal Galinstan (GaInSn) interconnections, as shown in Figure 6. The strain sensor could be driven by using the power stored in the supercapacitor. Figure 6a shows a schematic illustration and optical images of the integrated system with a circuit diagram. The integrated all-in-one textile system was sewn to a T-shirt and a nylon glove to monitor various biosignals. As shown in Figure S24, Cu wires (diameter: 0.1 mm) were utilized to link the all-in-one system sewn outside of the sleeve with analyzers. Two Cu wires were connected to electrochemical analyzer for charging the supercapacitor. Another two Cu wires were connected to measure the applied strain of the sensor by an amperemeter. After the supercapacitor was fully charged, the two Cu wires connected to the electrochemical analyzer were removed. Figure 6b shows the current change in accordance with precise tracking of a finger bending to different degrees detected by the system sewn on a nylon glove. Additionally, wrist bending could be distinguished, as shown in Figure 6c. We confirmed the current change of the strain sensor driven by a constant voltage of 1 V for finger and wrist bending motions (Figure S25), and the same patterns were observed as those detected with the sensor driven by the supercapacitor. The all-in-one system was sewn inside a glove to detect real-time wrist pulse signals under relaxation conditions (Figure 6d). The results clearly display repeatable and regular pulse shapes during relaxation with a frequency of 84 beats/min. As shown in the inset, the optical image and magnified graph of the pulse peak clearly reveal typical characteristics of the pulse waveform, such as the percussion wave (P-wave), tidal wave (T-wave), and diastolic wave (D-wave), demonstrating the high sensitivity of our system. Figure 6e shows the change in current for different elbow bending degrees monitored with the all-in-one system sewn to a T-shirt in the elbow area. A sharp change in the current due to the large strain applied by increasing the elbow bending angle was observed.

Figure S26a shows the detection of constant applied strain using the single supercapacitor as a power source for 2400 s. Because we could not keep the output voltage of the supercapacitor constant during the operation of the strain sensor, we measured the normalized current change ($\Delta I/I_0$), where I_0 and I are the current before and after application of strain in Figure S26b. $\Delta I/I_0$ remained constant when constant strain (10%) was applied, confirming the reliable operation of the sensor quantitatively. Figure S27 shows $\Delta I/I_0$ *versus* strain curve of the strain sensor, where the resistance value of Figure 5a is replaced with the current. Figure S26b is exactly matched with the data taken from the sensor with a 3 mL solution coating of Figure S27, where the strain sensor was driven by an external power supply. These results confirm that our all-in-one system detects the strain reliably for 40 min, corresponding to the strain measured with the same sensor but driven by the external constant power source. Basically, dramatically increasing the energy density of the supercapacitor by designing an asymmetric electrode or extra circuit to keep the output voltage of the supercapacitor constant would be the solution to longer operation of the sensor.[53,54]

Finally, we evaluate the effect of encapsulation on the device performance. Figure S28 compares the device performance upon encapsulation *via* sewing a fabric layer. Figure S28a

DOI: 10.1021/acsnano.9b04340
ACS Nano 2019, 13, 10469−10480

shows the optical image of the all-in-one system with an encapsulation layer. As shown in Figure S28b,c, respectively, there appears no change in the electrochemical performance of the supercapacitor and the sensitivity of the strain sensor after encapsulation process. Furthermore, we verify that the all-in-one system can detect the elbow bending as observed with the system without encapsulation (Figure S28d). It shows that the encapsulation can help to lengthen the lifetime of our devices by protecting them from external impact. These results demonstrate the excellent performance of our all-in-one textile system for monitoring of various human activities. In future studies, more functionalities, such as encapsulation for protection against sweat and energy harvesting for wireless charging of the supercapacitor, will be added to the all-in-one system for more practical wearable applications.

CONCLUSION

In this work, we proposed an all-in-one system consisting of a supercapacitor and a strain sensor based on a stretchable textile substrate for monitoring of biosignals. Both the supercapacitor and strain sensor were deliberately fabricated on a stretchable textile substrate; the former is in the course direction of the fabric with a small change in resistance, but the latter is in the wale direction with a large change in resistance under applied strain. By controlling the mixing ratio and amount of MWCNT/MoO_3 NW nanocomposite, the capacitance of the supercapacitor and the sensitivity of the strain sensor were maximized. After the supercapacitor and the strain sensor were integrated *via* the use of Galinstan liquid metal interconnections, the all-in-one system was sewn onto a T-shirt and a nylon glove to detect joint movements and subtle wrist pulses. This work demonstrates a facile fabrication process and application of the dynamically stretchable high-performance supercapacitor to power the integrated sensor in textile-based stretchable all-in-one systems for monitoring of biosignals while being worn for a long time without inconveniencing the user.

METHODS

Preparation of the Dispersed MWCNT Solution. MWCNTs (≥99 wt %, ≤13−18 nm outer diameter; Nano Integris) were refluxed in concentrated sulfuric acid and nitric acid (3:1 v/v; Sigma-Aldrich) at 70 °C for 3 h to prepare carboxylic-acid-functionalized MWCNTs (MWCNT−COOH). These functionalized MWCNTs were rinsed with DI water several times using a cellulose ester membrane filter (pore size 0.2 μm, diameter 47 mm; Advantec MFS, Inc.). After osmosis filtration with a tube cellulose membrane (average flat width 33 mm, average diameter 21 mm; Sigma), MWCNT−COOH was finally obtained. Finally, MWCNT−COOH was dispersed in ethanol (alcohol reagent, anhydrous, denatured, ACS, 94−96%; Alfa Aesar) (1 mg/mL).

Synthesis of Molybdenum Trioxide Nanowires (MoO_3 NWs). Molybdenum trioxide was synthesized *via* a hydrothermal method. Typically, 2 g of molybdenum powder (APS typically 2−4 μm, 99.9%; Alfa Aesar) was added into 10 mL of DI water to form a uniform mixture. Then, 20 mL of 30% (wt %) H_2O_2 was slowly added until the solution became light yellow (dark blue to light yellow). The solution was transferred to a Teflon-lined stainless-steel autoclave and heated to 220 °C for 12 h. The precipitate was filtered and rinsed several times with DI water and ethanol. The synthesized molybdenum trioxide NWs were dispersed in ethanol (0.5 mg/mL).

Fabrication of the Stretchable Conductive Fabric Substrate. MWCNT−COOH (1 mg/mL) and MoO_3 NWs (0.5 mg/mL) dispersed in ethanol were blended with various weight percent compositions. The blended nanocomposite solution was spray- coated on the stretchable fabric substrate (nylon (82%)/Spandex (18%)). The nanocomposite solution was spray-coated at a 90° angle above the substrate and 10 cm from the nozzle while the substrate was heated at 80 °C.

Preparation of the Organic Gel Electrolyte. The organic gel electrolyte consists of adding acetonitrile (ACN) (anhydrous, 99.8%; Sigma-Aldrich) and propylene carbonate (PC) (anhydrous, 99.7%; Sigma-Aldrich) using a syringe into a vial containing lithium perchlorate ($LiClO_4$) (battery grade, dry, 99.99%; Sigma-Aldrich). Then, poly(methyl methacrylate)(PMMA) (average $M_w \sim 996\,000$ by GPC, crystalline; Sigma-Aldrich) was slowly added into the solution to enhance the viscosity, and the mixture was heated at 70 °C for 6 h. The electrolyte has a weight percent composition of 39:39:7:15 (ACN/PC/$LiClO_4$/PMMA).

Fabrication of the Stretchable Fabric Supercapacitor. For the current collector, a PEDOT:PSS (Clevios PH1000) solution was mixed with 5 wt % of P123 (poly(ethylene glycol)-*block*-poly(propylene glycol)-*block*-poly(ethylene glycol) (M_n = ∼5800, PEO_{20}-PPO_{70}-PEO_{20}, Pluronic P123, P123) and stirred at 800 rpm overnight. The stretchable fabric substrate was dip-coated with the P123-modified PEDOT:PSS conductive composite solution to prepare the current collector of the supercapacitor. Then, the substrate was cured in an oven at 130 °C for 30 min. Subsequently, a MWCNT−COOH and MoO_3-NW-blended nanocomposite solution was spray-coated on the substrate, and the gel electrolyte was spread on the conductive fabric substrate. The two electrodes were then assembled together.

Characterizations. The surface morphology and textile structure of the MWCNTs, MoO_3 NWs, and MWCNT/MoO_3 nanocomposite were investigated by obtaining SEM (Hitachi S-4800 and Quanta 250 FEG) images. Raman spectra were obtained (Horiba LabRam Aramis IR2), and the wavelength of the laser and the power were 532 nm and 0.5 mW, respectively. X-ray diffraction (SmartLab, Rigaku) and X-ray photoelectron spectroscopy (X-TOOL-ULVAC, PHI) measurements were performed to investigate the chemical composition of the hydrothermally synthesized MoO_3 NWs. The electrochemical properties were obtained using CV, GCD, and electrochemical impedance spectroscopy with an electrochemical analyzer (Ivium Technologies, Compact Stat). The electrical characteristics of the strain sensor were measured using a probe station (Agilent Technologies B1500A).

Electrochemical Measurements and Calculations. To evaluate the electrochemical performance of the individual electrodes and fabricated stretchable supercapacitors, CV and GCD curves were obtained in a three-electrode cell and two-electrode cell using an electrochemical analyzer. In the three-electrode cell with 0.5 M Na_2SO_4 electrolyte, Ag/AgCl electrode, Pt wire, and an individual electrode were used as the reference, counter, and working electrodes, respectively. The capacitance of the cell (C_{cell}) was calculated from the GCD curves according to the following eq 4:

$$C_{electrode} = C_{cell} = \frac{i}{\left(\frac{dV}{dt}\right)} \tag{4}$$

where i and dV/dt correspond to the discharge current and the slope of the discharge curve, respectively. The specific capacitance of the cell ($C_{cell,s}$) was calculated using the relation $C_{cell,s} = C_{cell}/M_{cell}$, where M_{cell} is the mass loading of active material. The total mass of the active material of the MWNCT/MoO_3 nanocomposite was 1.4 mg. The projection area and volume of the supercapacitor were 2 cm^2 and 0.166 cm^3, respectively. The specific energy density ($E_{cell,s}$) and power density ($P_{cell,s}$) were calculated by the following eqs 5 and 6:

$$E_{cell,s} = \frac{C_{cell,s} \times \Delta V^2}{2 \times 3600} \tag{5}$$

$$P_{cell,s} = \frac{E_{cell,s} \times 3600}{t_{discharge}} \tag{6}$$

where ΔV is the voltage window and $t_{discharge}$ is the discharge time.

DOI: 10.1021/acsnano.9b04340
ACS Nano 2019, 13, 10469−10480

ASSOCIATED CONTENT

Supporting Information

The Supporting Information is available free of charge on the ACS Publications website at DOI: 10.1021/acsnano.9b04340.

Optical and SEM images of a fabric substrate; SEM images of dip-coated fabric; resistance change with dip-coating cycles; schematic of spray-coating conditions; SEM images of the fabric substrate before and after stretching; SEM images of course and wale direction stretching; SEM images of MWCNT/MoO_3-nanocomposite-coated fabric; shear viscosity of gel electrolyte; three-electrode electrochemical measurements; sheet resistance with the volume fractions of MoO_3 NWs; SEM images taken from the MWCNT/MoO_3 nanocomposite; relative resistance change with applied strain and resistance change of current collector with dip-coating cycles; relative resistance change with and without current collector and thickness of MWCNT/MoO_3 nanocomposite; adhesion test of coated materials; CV curves of gel electrolyte; CV curves, Nyquist plot, and volumetric capacitance of the supercapacitor; supercapacitor specifications; CV and self-discharge curve of the supercapacitor; temperature dependence of the supercapacitor; sheet resistance, relative resistance change, and thickness of the strain sensor; $I-V$ curve of MoO_3-NW-coated fabric; electrical characteristics with PDMS coating and washability; temperature dependence of the strain sensor; photograph of Cu wires; current change of the strain sensor driven by constant voltage applied; long time operation of all-in-one system; relative current change of strain sensor; photograph of the all-in-one system with encapsulation layer (PDF)

AUTHOR INFORMATION

Corresponding Author

*E-mail: jeongsha@korea.ac.kr.

ORCID

Jeong Sook Ha: 0000-0003-1358-3295

Notes

The authors declare no competing financial interest.

ACKNOWLEDGMENTS

This work was supported by the National Research Foundation of Korea (NRF) grant funded by the Korean government (MSIP) (Grant No. NRF-2019R1A2B5B03069545). It was also supported by a Korea University Grant. The authors also thank the KU-KIST graduate school program of Korea University.

REFERENCES

(1) Gao, W.; Emaminejad, S.; Nyein, H. Y. Y.; Challa, S.; Chen, K.; Peck, A.; Fahad, H. M.; Ota, H.; Shiraki, H.; Kiriya, D.; Lien, D.-H.; Brooks, G. A.; Davis, R. W.; Javey, A. Fully Integrated Wearable Sensor Arrays for Multiplexed *in situ* Perspiration Analysis. *Nature* **2016**, *529*, 509.

(2) Pu, X.; Li, L.; Song, H.; Du, C.; Zhao, Z.; Jiang, C.; Cao, G.; Hu, W.; Wang, Z. L. A Self-Charging Power Unit by Integration of a Textile Triboelectric Nanogenerator and a Flexible Lithium-Ion Battery for Wearable Electronics. *Adv. Mater.* **2015**, *27*, 2472−2478.

(3) Wang, Y.; Wang, L.; Yang, T.; Li, X.; Zang, X.; Zhu, M.; Wang, K.; Wu, D.; Zhu, H. Wearable and Highly Sensitive Graphene Strain Sensors for Human Motion Monitoring. *Adv. Funct. Mater.* **2014**, *24*, 4666−4670.

(4) Trung, T. Q.; Ramasundaram, S.; Hwang, B. U.; Lee, N. E. An All-Elastomeric Transparent and Stretchable Temperature Sensor for Body-Attachable Wearable Electronics. *Adv. Mater.* **2016**, *28*, 502−509.

(5) Wen, Z.; Yeh, M.-H.; Guo, H.; Wang, J.; Zi, Y.; Xu, W.; Deng, J.; Zhu, L.; Wang, X.; Hu, C.; Zhu, L.; Sun, X.; Wang, Z. L. Self-Powered Textile for Wearable Electronics by Hybridizing Fiber-Shaped Nanogenerators, Solar Cells, and Supercapacitors. *Sci. Adv.* **2016**, *2*, No. e1600097.

(6) Weng, W.; Chen, P.; He, S.; Sun, X.; Peng, H. Smart Electronic Textiles. *Angew. Chem., Int. Ed.* **2016**, *55*, 6140−6169.

(7) Heo, J. S.; Eom, J.; Kim, Y.-H.; Park, S. K. Recent Progress of Textile-Based Wearable Electronics: A Comprehensive Review of Materials, Devices, and Applications. *Small* **2018**, *14*, 1703034.

(8) Jung, S.; Lee, J.; Hyeon, T.; Lee, M.; Kim, D.-H. Fabric-Based Integrated Energy Devices for Wearable Activity Monitors. *Adv. Mater.* **2014**, *26*, 6329−6334.

(9) Wang, C.; Zhang, M.; Xia, K.; Gong, X.; Wang, H.; Yin, Z.; Guan, B.; Zhang, Y. Intrinsically Stretchable and Conductive Textile by a Scalable Process for Elastic Wearable Electronics. *ACS Appl. Mater. Interfaces* **2017**, *9*, 13331−13338.

(10) Liao, X.; Zhang, Z.; Kang, Z.; Gao, F.; Liao, Q.; Zhang, Y. Ultrasensitive and Stretchable Resistive Strain Sensors Designed for Wearable Electronics. *Mater. Horiz.* **2017**, *4*, 502−510.

(11) Hu, L.; Chen, W.; Xie, X.; Liu, N.; Yang, Y.; Wu, H.; Yao, Y.; Pasta, M.; Alshareef, H. N.; Cui, Y. Symmetrical MnO2−Carbon Nanotube−Textile Nanostructures for Wearable Pseudocapacitors with High Mass Loading. *ACS Nano* **2011**, *5*, 8904−8913.

(12) Pu, X.; Liu, M.; Li, L.; Han, S.; Li, X.; Jiang, C.; Du, C.; Luo, J.; Hu, W.; Wang, Z. L. Wearable Textile-Based In-Plane Microsupercapacitors. *Adv. Energy Mater.* **2016**, *6*, 1601254.

(13) Jost, K.; Stenger, D.; Perez, C. R.; McDonough, J. K.; Lian, K.; Gogotsi, Y.; Dion, G. Knitted and Screen Printed Carbon-Fiber Supercapacitors for Applications in Wearable Electronics. *Energy Environ. Sci.* **2013**, *6*, 2698−2705.

(14) Shen, C.; Xie, Y.; Zhu, B.; Sanghadasa, M.; Tang, Y.; Lin, L. Wearable Woven Supercapacitor Fabrics with High Energy Density and Load-Bearing Capability. *Sci. Rep.* **2017**, *7*, 14324.

(15) Chen, Y.; Xu, B.; Gong, J.; Wen, J.; Hua, T.; Kan, C.-W.; Deng, J. Design of High-Performance Wearable Energy and Sensor Electronics from Fiber Materials. *ACS Appl. Mater. Interfaces* **2019**, *11*, 2120−2129.

(16) Huang, Y.; Kershaw, S. V.; Wang, Z.; Pei, Z.; Liu, J.; Huang, Y.; Li, H.; Zhu, M.; Rogach, A. L.; Zhi, C. Highly Integrated Supercapacitor-Sensor Systems *via* Material and Geometry Design. *Small* **2016**, *12*, 3393−3399.

(17) Chen, J.; Wang, X.; Wang, J.; Lee, P. S. Sulfidation of NiMn-Layered Double Hydroxides/Graphene Oxide Composites toward Supercapacitor Electrodes with Enhanced Performance. *Adv. Energy Mater.* **2016**, *6*, 1501745.

(18) Yuan, L.; Yao, B.; Hu, B.; Huo, K.; Chen, W.; Zhou, J. Polypyrrole-Coated Paper for Flexible Solid-State Energy Storage. *Energy Environ. Sci.* **2013**, *6*, 470−476.

(19) Yang, Z.; Pang, Y.; Han, X.-l.; Yang, Y.; Ling, J.; Jian, M.; Zhang, Y.; Yang, Y.; Ren, T.-L. Graphene Textile Strain Sensor with Negative Resistance Variation for Human Motion Detection. *ACS Nano* **2018**, *12*, 9134−9141.

(20) Chen, S.; Liu, S.; Wang, P.; Liu, H.; Liu, L. Highly Stretchable Fiber-Shaped E-Textiles for Strain/Pressure Sensing, Full-Range Human Motions Detection, Health Monitoring, and 2D Force Mapping. *J. Mater. Sci.* **2018**, *53*, 2995−3005.

(21) Shakir, I.; Shahid, M.; Cherevko, S.; Chung, C.-H.; Kang, D. J. Ultrahigh-Energy and Stable Supercapacitors Based on Intertwined Porous MoO_3−MWCNT Nanocomposites. *Electrochim. Acta* **2011**, *58*, 76−80.

DOI: 10.1021/acsnano.9b04340
ACS Nano 2019, 13, 10469−10480

(22) Brezesinski, T.; Wang, J.; Tolbert, S. H.; Dunn, B. Ordered Mesoporous α-MoO_3 with Iso-Oriented Nanocrystalline Walls for Thin-Film Pseudocapacitors. *Nat. Mater.* **2010**, *9*, 146.
(23) Wang, J.; Xue, P.; Tao, X.; Yu, T. Strain Sensing Behavior and Its Mechanisms of Electrically Conductive PPy-Coated Fabric. *Adv. Eng. Mater.* **2014**, *16*, 565−570.
(24) Dong, K.; Wang, Y.-C.; Deng, J.; Dai, Y.; Zhang, S. L.; Zou, H.; Gu, B.; Sun, B.; Wang, Z. L. A Highly Stretchable and Washable All-Yarn-Based Self-Charging Knitting Power Textile Composed of Fiber Triboelectric Nanogenerators and Supercapacitors. *ACS Nano* **2017**, *11*, 9490−9499.
(25) Lee, H.; Glasper, M. J.; Li, X.; Nychka, J. A.; Batcheller, J.; Chung, H.-J.; Chen, Y. Preparation of Fabric Strain Sensor Based on Graphene for Human Motion Monitoring. *J. Mater. Sci.* **2018**, *53*, 9026−9033.
(26) Xu, W.; Yang, T.; Qin, F.; Gong, D.; Du, Y.; Dai, G. A Sprayed Graphene Pattern-Based Flexible Strain Sensor with High Sensitivity and Fast Response. *Sensors* **2019**, *19*, 1077.
(27) Jang, Y.; Jo, J.; Woo, K.; Lee, S.-H.; Kwon, S.; Kim, K.-Y.; Kang, D. 2D All-Solid State Fabric Supercapacitor Fabricated *via* An All Solution Process for Use in Smart Textiles. *Appl. Phys. Lett.* **2017**, *110*, 203902.
(28) Park, H.; Kim, D. S.; Hong, S. Y.; Kim, C.; Yun, J. Y.; Oh, S. Y.; Jin, S. W.; Jeong, Y. R.; Kim, G. T.; Ha, J. S. A Skin-Integrated Transparent and Stretchable Strain Sensor with Interactive Color-Changing Electrochromic Displays. *Nanoscale* **2017**, *9*, 7631−7640.
(29) Lv, Z.; Luo, Y.; Tang, Y.; Wei, J.; Zhu, Z.; Zhou, X.; Li, W.; Zeng, Y.; Zhang, W.; Zhang, Y.; Qi, D.; Pan, S.; Loh, X. J.; Chen, X. Editable Supercapacitors with Customizable Stretchability Based on Mechanically Strengthened Ultralong MnO_2 Nanowire Composite. *Adv. Mater.* **2018**, *30*, 1704531.
(30) Stassi, S.; Cauda, V.; Canavese, G.; Pirri, C. F. Flexible Tactile Sensing Based on Piezoresistive Composites: A Review. *Sensors* **2014**, *14*, 5296−5332.
(31) Atalay, O.; Kennon, W. R.; Demirok, E. Weft-Knitted Strain Sensor for Monitoring Respiratory Rate and Its Electro-Mechanical Modeling. *IEEE Sens. J.* **2015**, *15*, 110−122.
(32) Wang, J.; Long, H.; Soltanian, S.; Servati, P.; Ko, F. Electromechanical Properties of Knitted Wearable Sensors: Part 1 − Theory. *Text. Res. J.* **2014**, *84*, 3−15.
(33) Atalay, O.; Kennon, W. Knitted Strain Sensors: Impact of Design Parameters on Sensing Properties. *Sensors* **2014**, *14*, 4712.
(34) Wang, C.; Xia, K.; Jian, M.; Wang, H.; Zhang, M.; Zhang, Y. Carbonized Silk Georgette as an Ultrasensitive Wearable Strain Sensor for Full-Range Human Activity Monitoring. *J. Mater. Chem. C* **2017**, *5*, 7604−7611.
(35) Atalay, O.; Kennon, W.; Husain, M. Textile-Based Weft Knitted Strain Sensors: Effect of Fabric Parameters on Sensor Properties. *Sensors* **2013**, *13*, 11114.
(36) Arasu, P. A.; Williams, R. V. The Dielectric Studies on Sol−Gel Routed Molybdenum Oxide Thin Film. *J. Adv. Dielectr.* **2017**, *07*, 1750011.
(37) Chen, Y.; Lu, C.; Xu, L.; Ma, Y.; Hou, W.; Zhu, J.-J. Single-Crystalline Orthorhombic Molybdenum Oxide Nanobelts: Synthesis and Photocatalytic Properties. *CrystEngComm* **2010**, *12*, 3740−3747.
(38) Mane, A. A.; Nikam, S. A.; Moholkar, A. V. NO2 Gas Sensing Properties of Sprayed Composite Porous MoO3-V2O5 Thin Films. *Mater. Chem. Phys.* **2018**, *216*, 294−304.
(39) Zhou, K.; Zhou, W.; Liu, X.; Sang, Y.; Ji, S.; Li, W.; Lu, J.; Li, L.; Niu, W.; Liu, H.; Chen, S. Ultrathin MoO3 Nanocrystalsself-Assembled on Graphene Nanosheets *via* Oxygen Bonding as Supercapacitor Electrodes of High Capacitance and Long Cycle Life. *Nano Energy* **2015**, *12*, 510−520.
(40) Nakayama, M.; Tanaka, A.; Sato, Y.; Tonosaki, T.; Ogura, K. Electrodeposition of Manganese and Molybdenum Mixed Oxide Thin Films and Their Charge Storage Properties. *Langmuir* **2005**, *21*, 5907−5913.
(41) Lee, G.; Kim, D.; Kim, D.; Oh, S.; Yun, J.; Kim, J.; Lee, S.-S.; Ha, J. S. Fabrication of a Stretchable and Patchable Array of High Performance Micro-Supercapacitors Using a Non-Aqueous Solvent Based Gel Electrolyte. *Energy Environ. Sci.* **2015**, *8*, 1764−1774.
(42) Keum, K.; Lee, G.; Lee, H.; Yun, J.; Park, H.; Hong, S. Y.; Song, C.; Kim, J. W.; Ha, J. S. Wire-Shaped Supercapacitors with Organic Electrolytes Fabricated *via* Layer-by-Layer Assembly. *ACS Appl. Mater. Interfaces* **2018**, *10*, 26248−26257.
(43) Yun, T. G.; Kim, D.; Kim, Y. H.; Park, M.; Hyun, S.; Han, S. M. Photoresponsive Smart Coloration Electrochromic Supercapacitor. *Adv. Mater.* **2017**, *29*, 1606728.
(44) Hare, D. E.; Dlott, D. D. Picosecond Coherent Raman Study of Solid-State Chemical Reactions During Laser Polymer Ablation. *Appl. Phys. Lett.* **1994**, *64*, 715−717.
(45) Lee, G.; Kim, J. W.; Park, H.; Lee, J. Y.; Lee, H.; Song, C.; Jin, S. W.; Keum, K.; Lee, C.-H.; Ha, J. S. Skin-Like, Dynamically Stretchable, Planar Supercapacitors with Buckled Carbon Nanotube/Mn−Mo Mixed Oxide Electrodes and Air-Stable Organic Electrolyte. *ACS Nano* **2019**, *13*, 855−866.
(46) Chen, J.; Han, S.; Zhao, H.; Bai, J.; Wang, L.; Sun, G.; Zhang, Z.; Pan, X.; Zhou, J.; Xie, E. Robust Wire-Based Supercapacitors Based on Hierarchical α-MoO_3 Nanosheet Arrays with Well-Aligned Laminated Structure. *Chem. Eng. J.* **2017**, *320*, 34−42.
(47) Ye, L.; Liang, Q.; Huang, Z.-H.; Lei, Y.; Zhan, C.; Bai, Y.; Li, H.; Kang, F.; Yang, Q.-H. A Supercapacitor Constructed with a Partially Graphitized Porous Carbon and Its Performance Over a Wide Working Temperature Range. *J. Mater. Chem. A* **2015**, *3*, 18860−18866.
(48) Jeong, Y. R.; Park, H.; Jin, S. W.; Hong, S. Y.; Lee, S.-S.; Ha, J. S. Highly Stretchable and Sensitive Strain Sensors Using Fragmentized Graphene Foam. *Adv. Funct. Mater.* **2015**, *25*, 4228−4236.
(49) Seyedin, S.; Zhang, P.; Naebe, M.; Qin, S.; Chen, J.; Wang, X.; Razal, J. M. Textile Strain Sensors: A Review of the Fabrication Technologies, Performance Evaluation and Applications. *Mater. Horiz.* **2019**, *6*, 219−249.
(50) Mattmann, C.; Clemens, F.; Tröster, G. Sensor for Measuring Strain in Textile. *Sensors* **2008**, *8*, 3719−3732.
(51) Chithambararaj, A.; Rajeswari Yogamalar, N.; Bose, A. C. Hydrothermally Synthesized h-MoO_3 and α-MoO_3 Nanocrystals: New Findings on Crystal-Structure-Dependent Charge Transport. *Cryst. Growth Des.* **2016**, *16*, 1984−1995.
(52) Benchirouf, A.; Palaniyappan, S.; Ramalingame, R.; Raghunandan, P.; Jagemann, T.; Müller, C.; Hietschold, M.; Kanoun, O. Electrical Properties of Multi-Walled Carbon Nanotubes/PEDOT:PSS Nanocomposites Thin Films Under Temperature and Humidity Effects. *Sens. Actuators, B* **2016**, *224*, 344−350.
(53) Jiang, Q.; Kurra, N.; Alhabeb, M.; Gogotsi, Y.; Alshareef, H. N. All Pseudocapacitive MXene-RuO_2 Asymmetric Supercapacitors. *Adv. Energy Mater.* **2018**, *8*, 1703043.
(54) Kim, D.; Kim, D.; Lee, H.; Jeong, Y. R.; Lee, S.-J.; Yang, G.; Kim, H.; Lee, G.; Jeon, S.; Zi, G.; Kim, J.; Ha, J. S. Body-Attachable and Stretchable Multisensors Integrated with Wirelessly Rechargeable Energy Storage Devices. *Adv. Mater.* **2016**, *28*, 748−756.

DOI: 10.1021/acsnano.9b04340
ACS Nano 2019, 13, 10469−10480